

Seismic site characterization for Moulvibazar town, Bangladesh

Md. Zillur Rahman¹ · Md. Shakhawat Hossain² · A. S. M. Maksud Kamal² · Sumi Siddiqua¹  · Fansab Mustahid² · Atikul Haque Farazi³

Received: 28 October 2016 / Accepted: 7 March 2017 / Published online: 17 March 2017
© Springer-Verlag Berlin Heidelberg 2017

Abstract In recent years, decision-making and site-planning strategies for earthquake mitigation have shifted away from a crisis management approach, to a greater emphasis on risk reduction. The earthquake hazard of a particular area can be assessed using geophysical and geotechnical site investigations. In the present study, seismic site characterization was carried out to evaluate earthquake risk for the town of Moulvibazar, Bangladesh, by integrating geophysical and geotechnical approaches. The study revealed that the average shear wave velocity to a depth of 30 m (AVS30) varied from 150 to 235 m/s, and US National Earthquake Hazards Reduction Program (NEHRP) soil site classes D and E were predominant, with soil amplification factors (SAF) of 1.3 and 1.45 for site classes D and E, respectively. In addition, peak ground acceleration (PGA) at the ground surface ranged from 0.325 to 0.3625 g, foundation layer depths for the deep foundation varied from 15 to 29 m, and the predominant periods ranged from 0.35 to 0.72 s. These soil parameters can be used to prepare an earthquake risk-sensitive land use plan for future urban development and to design earthquake-resistant structures.

Keywords Seismic site characterization · AVS30 · PS logging · MASW · SPT-N · Predominant period

Introduction

Seismic site characterization is the primary component in seismic risk management and seismic design of structures. Historical records of earthquakes indicate that several large-magnitude earthquake events occurred in northeastern India and Bangladesh as a result of ongoing tectonic deformation along the plate boundaries and active faults (Bilham 2004; Bilham and Hough 2006; Steckler et al. 2008; Morino et al. 2011, 2014; Rahman et al. 2015). Bangladesh, which covers the northeastern part of the Indian Plate, is located near the convergence plate boundaries between the Indian and Eurasian plates (Steckler et al. 2008). Bilham and England (2001) reported that seismic risk in northern Bangladesh had increased as a result of active deformation of the plateau pop-up structure at the location of the great Assam earthquake of 1897 in the northern margin of the Shillong Plateau in India. Although Bangladesh is located near one of the highest seismic risk zones in the world, a proper scenario of earthquake risk and related strategies, policies, and action plans regarding provisions, response, and recovery has not yet been formulated. Therefore, an integrated geophysical and geotechnical site characterization is necessary for the seismically vulnerable cities and towns in Bangladesh in order to enable seismic risk assessment and design of structures. In the present study, several geophysical and geotechnical site investigation techniques were used for seismic site characterization for the town of Moulvibazar, which is located close to the epicenter of the Srimangal Earthquake of 1918 (Fig. 1). The town is the capital of the district of Moulvibazar, located in northeastern Bangladesh. The 1918 Srimangal Earthquake ($M_w = 7.4$) caused massive damage to structures in the Srimangal Tea Estate

✉ Sumi Siddiqua
sumi.siddiqua@ubc.ca

¹ School of Engineering, The University of British Columbia, Okanagan Campus, Kelowna, BC V1V 1V7, Canada

² Department of Disaster Science and Management, University of Dhaka, Dhaka, Bangladesh

³ Department of Geology and Mining, University of Barisal, Barisal, Bangladesh

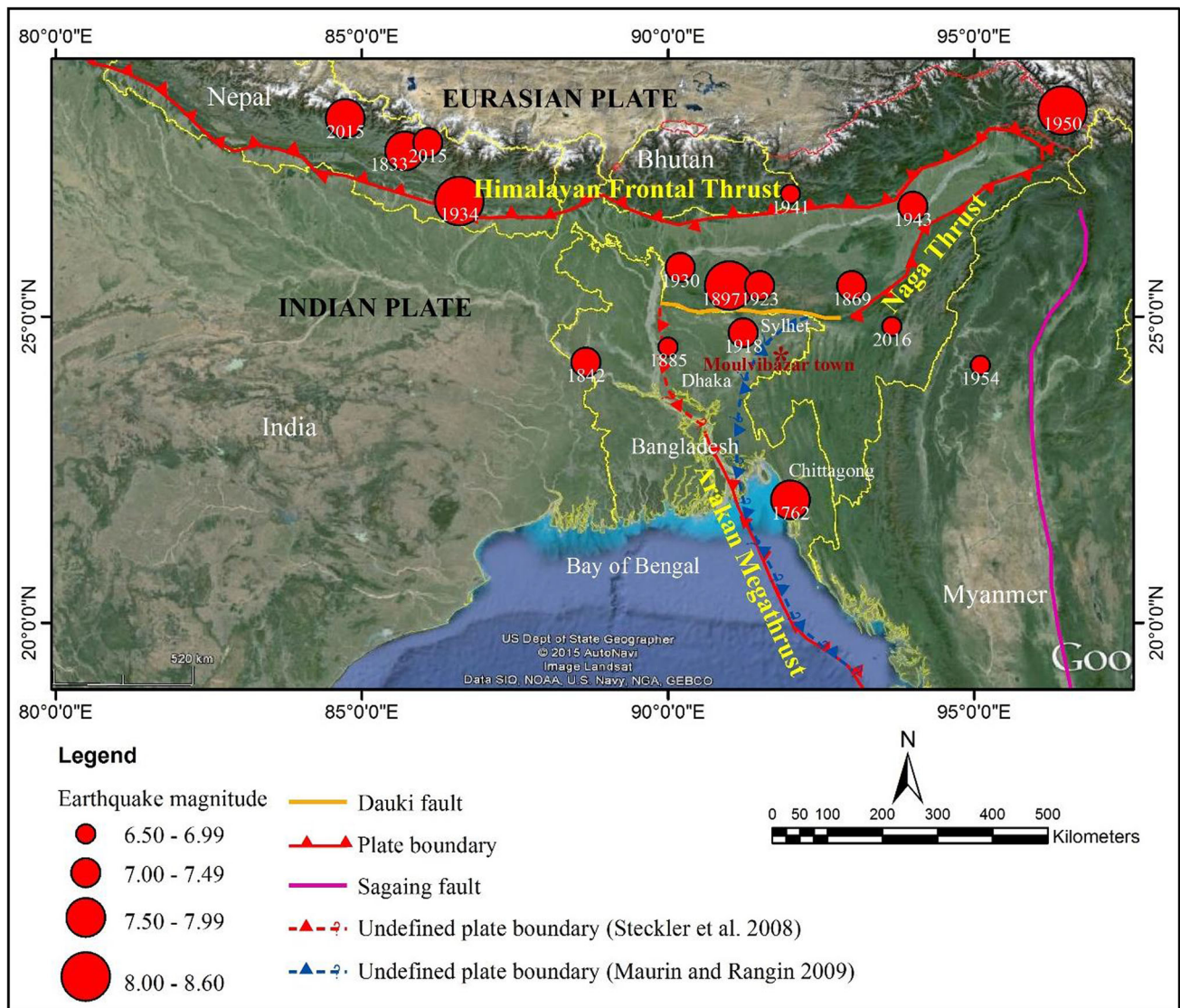


Fig. 1 Historical and recent earthquakes (magnitude ≥ 6.5) from 1762 to 2016. Historical earthquake locations and magnitudes are from Ambraseys and Douglas (2004) and Szeliga et al. (2010). Recent earthquake locations and magnitudes are from the United States

Geological Survey (USGS). The plate boundaries and faults are according to Maurin and Rangin (2009) and Steckler et al. (2008). The background map is from Google Earth

areas and the towns of Moulvibazar and Habiganj, which were located very close to the epicenter (Stuart 1920).

The amplification of ground motion in the near-surface soft soils overlying the base rock is largely responsible for the increased damage during a large earthquake (Anderson et al. 1996; Eker et al. 2012; Kuo et al. 2012). For seismic site characterization, recent building codes recommend using the average shear wave velocity of the near-surface soils down to a depth of 30 m (AVS30) for estimating the amplification factor of seismic ground motion during an earthquake (Borcherdt 1994; UBC 1997; Dobry et al. 2000; BSSC 2015). The Next Generation Attenuation of Ground Motion (NGA) project conducted by the Pacific Earthquake Engineering Research Center (PEER) used the AVS30 for

modeling ground motion attenuation (Abrahamson et al. 2013; Boore et al. 2013; Campbell and Bozorgnia 2013; Chiou and Youngs 2013). Table 1 presents the AVS30-based soil classification according to the National Earthquake Hazards Reduction Program (NEHRP, USA) for estimating the amplification factors of the seismic ground motion. Therefore, seismic site characterization is typically carried out using in situ site investigations and laboratory tests of samples to estimate the dynamic properties of soils for site response analysis and seismic microzonation (Park et al. 1999; Cavallaro et al. 2006; Hasançebi and Ulusay 2007; Benjumea et al. 2008; Cavallaro et al. 2008; Brandenberg et al. 2010; Kuo et al. 2011; Castelli et al. 2016; Rahman et al. 2016).

Table 1 National Earthquake Hazards Reduction Program (NEHRP) 1994 (BSSC 1994) AVS30-based site classification for seismic site response

Classification	AVS30 (m/s)	General description
A	AVS30 > 1500	Hard rock
B	1500 > AVS30 > 760	Firm to hard rock
C	760 > AVS30 > 360	Dense soil and soft rock
D	360 > AVS30 > 180	Stiff soil
E	180 > AVS30	Soft soil

In the present study, logging of compressional (primary) and shear (secondary) wave velocities (PS), multichannel analysis of surface waves (MASW), standard penetration test blow counts (SPT-N), and single microtremor (H/V) measurements were used to characterize the near-surface soils in the town of Moulvibazar in order to estimate the amplification factors of seismic ground motion.

Geomorphology and surface geology

The study area is characterized by relatively flat terrain comprising predominantly of floodplain deposits with low terraces in the southeast (Fig. 2). A surface geological map of the area exemplifies the physiographic features of the terrain and also reveals the geological attributes. The surface geological map units are the litho-genetic units that ultimately reflect the surface lithology as well as the physical processes involved in the geological evolution of

the study area. Table 2 depicts the surface geological (geomorphological) classification of the study area based on litho-genetic category, with a brief lithological description.

The investigated area consists of the floodplain of the Manu River, with conspicuous geomorphological as well as geographical features. Details of the map units are described in the following sections.

Active channel

In the present study area, the point bars are the main geomorphic features in the active channel.

Point bar deposit

A point bar deposit, which is a crescent-shaped sandy deposit having a gentle slope towards the riverbed, is situated on the convex side of a meandering loop that originated due to the action of lateral migration of a meandering river during flooding. Sediments formed primarily by the active channel processes are grouped in this class. Despite the different map units in the active channel litho-genetic category, the present study area is characterized only by point bar deposits. In the investigated area, a point bar sequence was identified in the Manu River (Fig. 2). The point bar shows a fining-upward sequence dominated by sand and silty sand in the lower portion, with the upper portion exhibiting clayey silt with silty clay deposits. Cross-bedding is a conspicuous sedimentary structure of this unit.

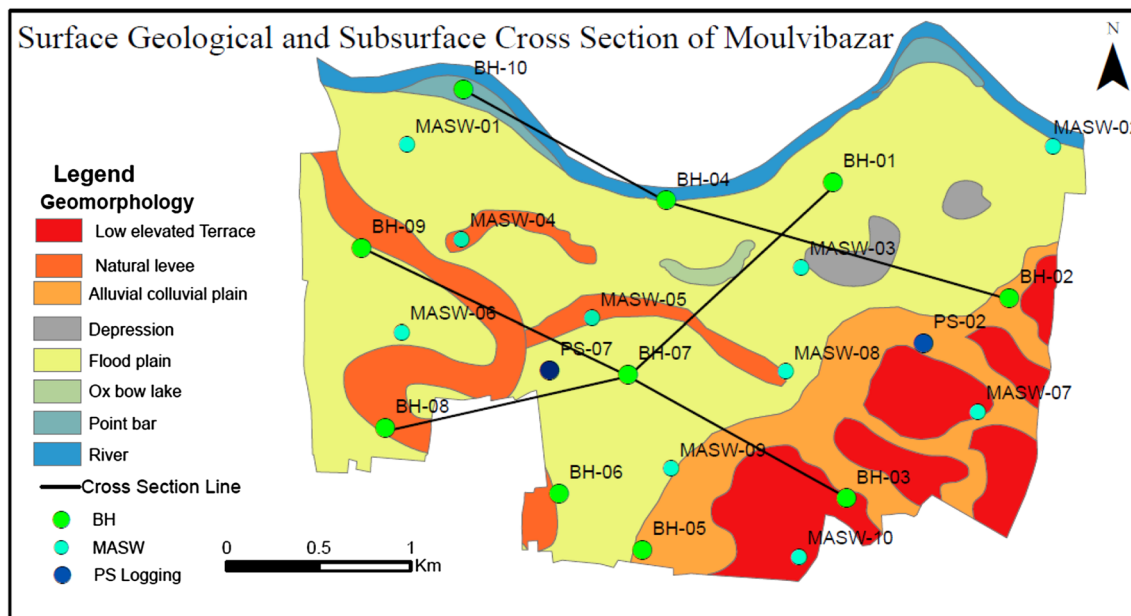


Fig. 2 Surface geological map units that reveal the surface geomorphology, and locations of the SPT boreholes (e.g., BH-01), PS logging (e.g., PS-02), and multichannel analysis of surface waves

(e.g., MASW-01), along with three cross-sections, used to explore the subsurface geological conditions of the study area

Table 2 Surface geological map units and lithological characteristics for each unit in the study area

Litho-genetic category	Map unit	Lithology
Active channel	Point bar deposit	Silty sand: yellowish brown, very fine-grained, root and rootlets; sand: light grey to brownish yellow, very fine- to medium-grained, and composed of quartz, mica, feldspar, and dark minerals
Overbank	Floodplain deposit	Silty clay, clayey silt, and sand: pale brown to grayish brown, medium- to very fine-grained, well sorted, and composed of quartz, feldspar, mica, and dark minerals
	Natural levee deposit	Clay, clayey silt, silty clay, silty sand, and sand: light gray to yellowish brown, medium- to very fine-grained, and composed of quartz, mica, dark minerals, and feldspar
	Oxbow lake deposit	Sandy silt with clay: staining pale brown to grayish brown, root and root-lets; silty clay to clayey silt: brown to dark gray, moderate stickiness and plasticity; sand: dark gray, medium- to fine-grained, and composed of quartz, mica, dark minerals, and feldspar
	Depression deposit	Silty clay and clayey silt: pale to yellowish brown, high stickiness and plasticity, with vegetal matter, huge patches
Terrace	Low terrace deposit	Clayey silt to silty clay with sand: mottling between red to yellowish red and light grey, presence of a concretionary bed of manganese and ferruginous nodules
	Alluvial-colluvial deposit	Silty clay and clayey silt, mixed with sand: patches between dark brown to yellowish brown and light grey. The mottling is red, and concretionary ferruginous nodules are the size of pebbles; sand: fine- to medium-grained, and composed of quartz, dark minerals, mica, and feldspar

Overbank

The map units related to the overbank depositional units are formed due to the overtopping of flood water. The units are described under four subheadings.

Floodplain deposit

A floodplain is an area located in close proximity to a river. The floodplain, which stretches from the bank of its main channel to the base of the enclosing valley wall, eventually experiences flooding during periods of high discharge. The investigated area comprises the Manu River floodplain (Fig. 2). Floodplain deposits adjacent to the active channel are predominantly pale brown to grayish brown clayey silt with occasional fine sand layers, while the distal floodplain sediments are silty clay to clayey silt of the same color. The deposits of older floodplains are characterized by light olive brown to olive and brownish yellow to yellowish brown staining along with root traces and root tubes.

Natural levee deposit

A narrow, elongated ridge running parallel to a channel or meander scar merging with the floodplain is known as a natural levee. Natural levees identified in the study area are mostly areas of human settlement and were modified by human activity (Fig. 2). However, they are sparsely distributed and the least developed. The lithology of the natural levees in the study area is predominantly clayey silt to silty sand, with successive interbedding of fine sand, silty sand, and sand.

Depression deposit

A depression is oval-shaped lowland with a permanent or seasonal water body that is observed within the floodplain. This particular map unit was not frequently observed spatially in the study area, since the studied terrain belongs to a relatively older floodplain or the whole area has been modified by human intervention. Depression deposits are developed far from a river (Fig. 2). During flood times, sediments settle over the floodplain and depression. The dominant lithology is pale to yellowish brown silty clay with high stickiness and plasticity, vegetal matter, and huge patches. However, clayey silt is also observed intercalated with the main lithological constituents.

Oxbow lake deposit

An oxbow lake is a U-shaped water body that is formed due to a meander cut-off during episodic flooding. Although it was somewhat difficult to differentiate whether this map unit was an oxbow lake or abandoned channel, its curved shape resembles that of a lake, thus suggesting an oxbow lake deposit (Fig. 2). Silty clay is the dominant lithology, and clayey silt with fine sand is also reported in this map unit.

Terrace

The terrace deposits are older in comparison to the active channel and overbank deposits. In general, the terraces are not inundated during normal flooding. They are divided into two units, which are described in the following sections.

Low terrace deposit

The low terrace deposits, which constitute the southern and southeastern part of the investigated area, display distinct map units that are completely different from the alluvial deposits in the remainder of the area. The area at higher elevation is dissected by numerous narrow to wide and shallow to moderately deep gullies, eventually activated by rainwater during the wet season. It is also traversed by small rainwater- and floodwater-fed ephemeral channels. The internal drainage network of these elevated terraces and depressions and external floodwater inlets gives rise to a unique depositional environment comprising both alluvial and colluvial sediments. The main lithological constituents are clayey silt to silty clay with sand, with mottling between red to yellowish red and light gray, and the presence of a concretionary bed of manganese and ferruginous nodules.

Alluvial-colluvial deposit

The alluvial-colluvial plains are basically the piedmont plains that lie between the hills, forming a wide fan-shaped body. The foothill piedmont deposits, which are linear bodies lying above the floodplain, are sloping gradually away from the hills (Fig. 2). The eroded terrace deposits, which are carried down by rainwater, are reworked and redeposited in the valleys as piedmont alluvial-colluvial deposits. During flash flooding, the piedmont deposits are never submerged in water. Thus, their sedimentation characteristics are somewhat different from those of the floodplain deposits. Most of the sediments are slope wash from hillsides, which are carried down and redeposited due to slope break. The sediments comprise mainly silty clay and clayey silt mixed with sand. Patches of color vary from pale to dark brown; however, few parts exhibit a mixed color combination. Pebble-sized ferruginous transported concretions and nodules are also present in this unit.

Subsurface geology

Lithological succession encountered in the boreholes reveals that the study area encompasses eight distinct lithofacies, denoted as layers (Figs. 3, 4, 5). Three cross-section profiles were prepared to elucidate the subsurface geological conditions of the study area. Each layer has distinct lithological characteristics and standard penetration test blow counts (SPT-N). Several boreholes to depths greater than 20 m were carefully examined to delineate the spatial distribution of the subsurface lithological units of the area.

Among the three cross-sections, two were drawn in a northwest–southeast direction along the floodplain of the Manu River, and the third was drawn in a northeast–southwest

direction across the floodplain. Cross-section 1 shows a consistent layer distribution throughout the section, which passes through the floodplain areas (Figs. 2, 3). The section is about 3 km in length, which is represented using three borehole logs, and comprises eight distinct geological layers.

Cross-section 2, with total length of 3 km, begins in the northwest and ends in the southeast of the study area (Figs. 2, 4). The section in the northwest belongs to the floodplain areas, whereas in the southeast the profile merges with the terrace. The section consists of seven distinct geological layers.

Cross-section 3 is about 2.5 km long, beginning in the northeast and ending in the southwest (Figs. 2, 5). The section, which comprises eight distinct geological layers, passes across the floodplain areas.

Seismotectonics

The study area is part of the Bengal Basin, one of the largest sedimentary basins in the world. Bangladesh covers a major portion of this basin (Alam et al. 2003). The northward collision of the Indian Plate with the Eurasian Plate created the Himalayan ranges and subsequent generation of a huge river network that forms the Bengal Basin in the eastern part of the Indian Plate (Curry et al. 1982; Acharyya 2007; Aitchison et al. 2007). Because of the complex interactions of the Eurasian, Indian, and Burma plates, Bangladesh is surrounded by plate boundaries in the north and east (Steckler et al. 2008; Maurin and Rangin 2009). Apart from these plate boundaries, the Dauki fault, which is considered the source of the 1897 great Assam earthquake (Oldham 1899), is located in the northern boundary of Bangladesh (Figs. 1, 6). Historically, several large-magnitude earthquakes have occurred along the plate boundaries and faults in northeastern India and Bangladesh (Ambraseys and Douglas 2004; Martin and Szeliga 2010; Szeliga et al. 2010). The 1918 Srimangal Earthquake was the most devastating earthquake for the town of Moulvibazar. A number of earthquakes with magnitudes of 5 to 6 have also occurred within the Bangladesh territory in the recent past. The seismicity of Bangladesh and surroundings from 1908 to 2016 is shown in Fig. 6.

Bangladesh is divided into three seismic zones based on peak ground acceleration (PGA) (BNBC 1993), with PGA values of 0.075, 0.15, and 0.25 g for zones I, II, and III, respectively (Fig. 7). Moulvibazar town is situated in Zone III.

Methodology

The 1997 NEHRP and Uniform Building Code (UBC) provision recommendations advised the use of average near-surface shear wave velocity of soils down to a depth

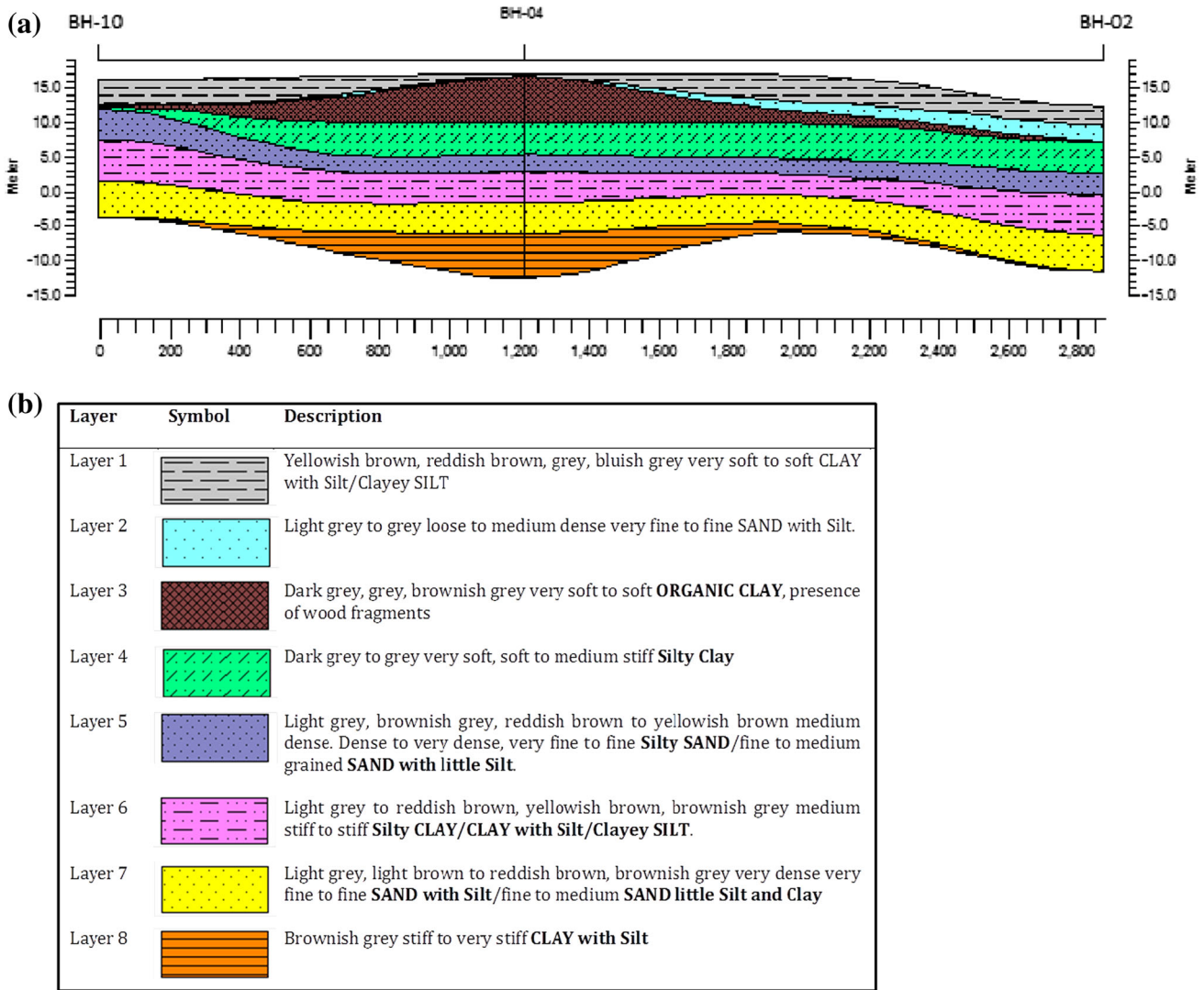


Fig. 3 a Lithological cross-section 1 along a line through locations BH-10, BH-04, and BH-02; b legend of the geological layers, with lithological symbol and description

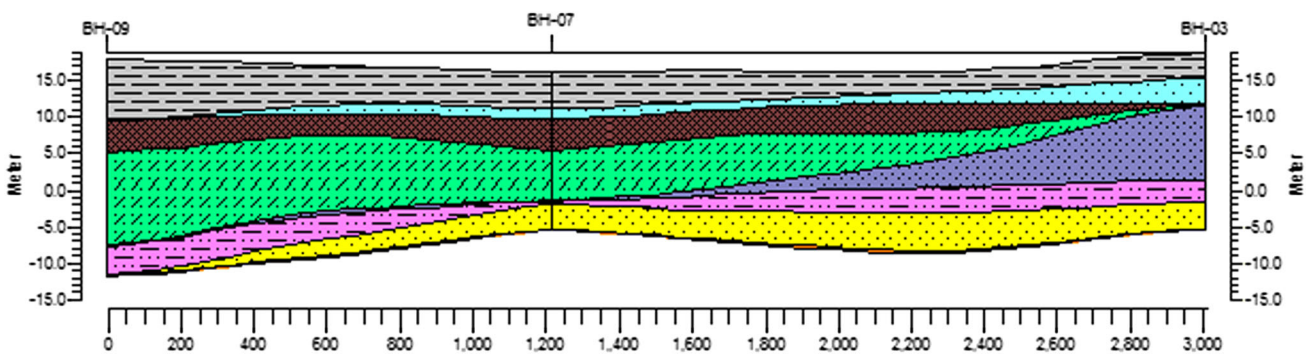


Fig. 4 Lithological cross-section 2 along a line through locations BH-09, BH-07, and BH-03 in Fig. 2. For the legend of the geological layers, refer to Fig. 3b

of 30 m (AVS30) as a parameter for seismic site characterization (Dobry et al. 2000). The near-surface shear wave velocity (V_s) of soils can be estimated using several in situ

site investigation techniques, including PS logging (downhole seismic), spectral analysis of surface waves (SASW), active and passive multichannel analysis of

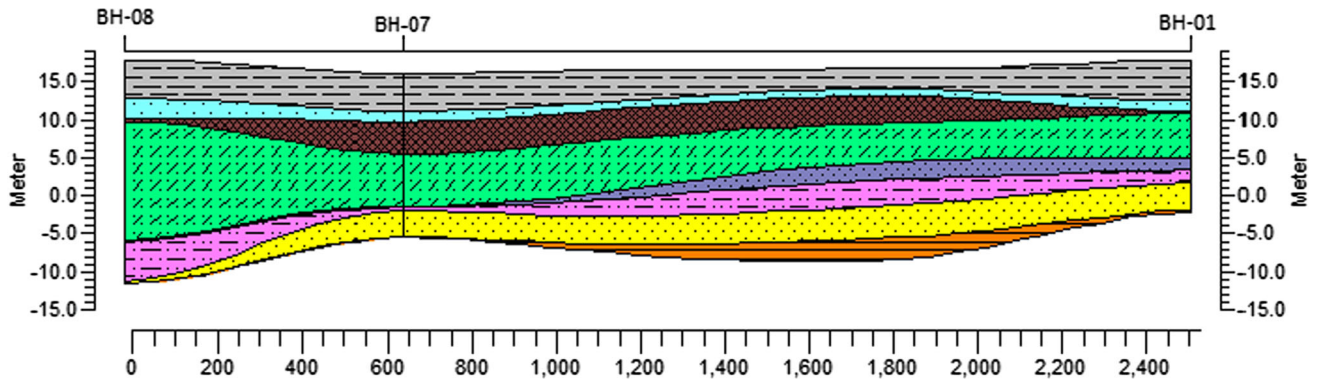


Fig. 5 Lithological cross-section 3 along a line through locations BH-08, BH-07, and BH-01 in Fig. 2. For the legend of the geological layers, refer to Fig. 3b

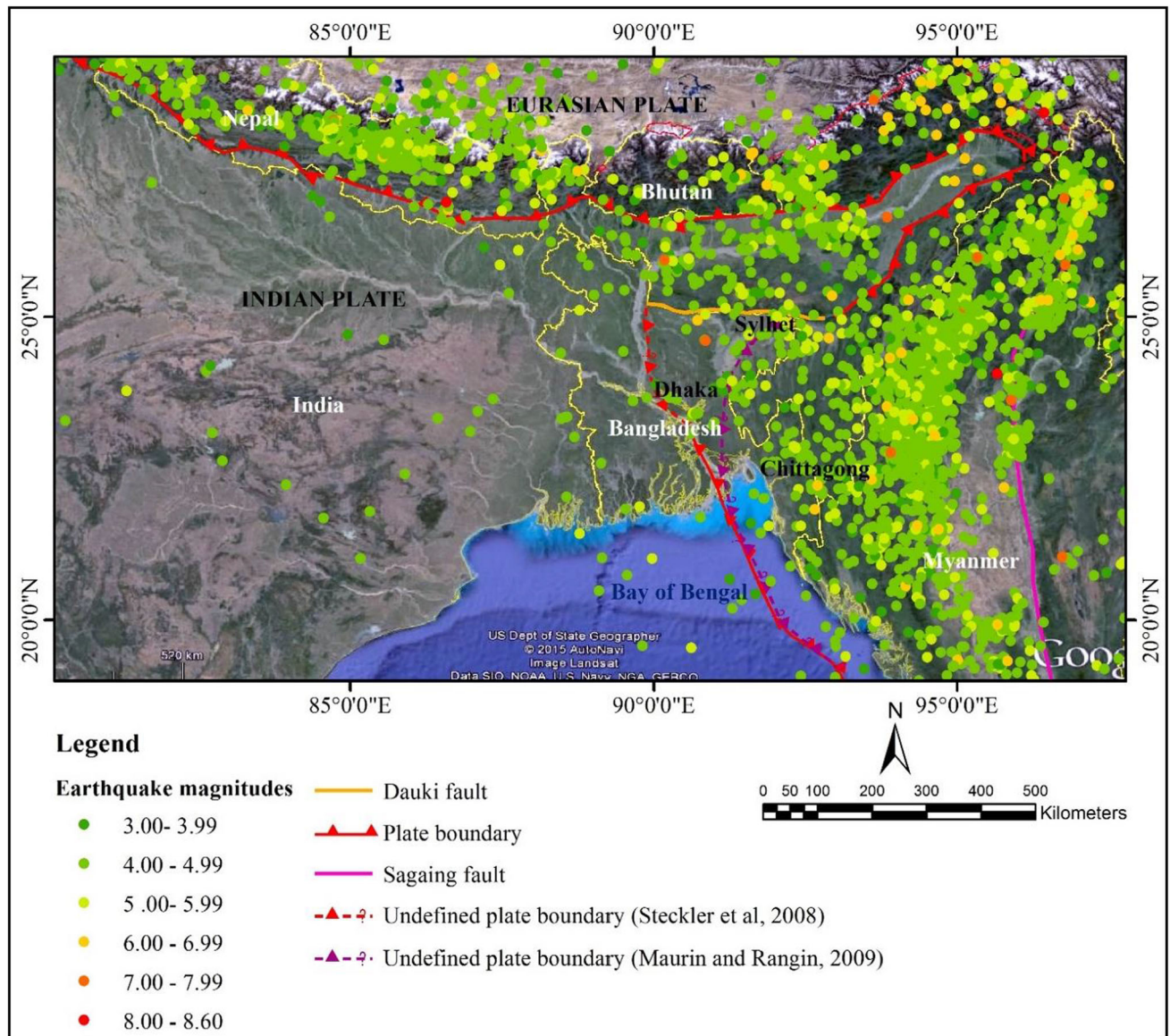


Fig. 6 Earthquakes (magnitude ≥ 3) that occurred from 1908 to 2015 in Bangladesh and surroundings, according to the earthquake catalogue from the United States Geological Survey. The plate boundaries and faults are according to Maurin and Rangin (2009) and Steckler et al. (2008)

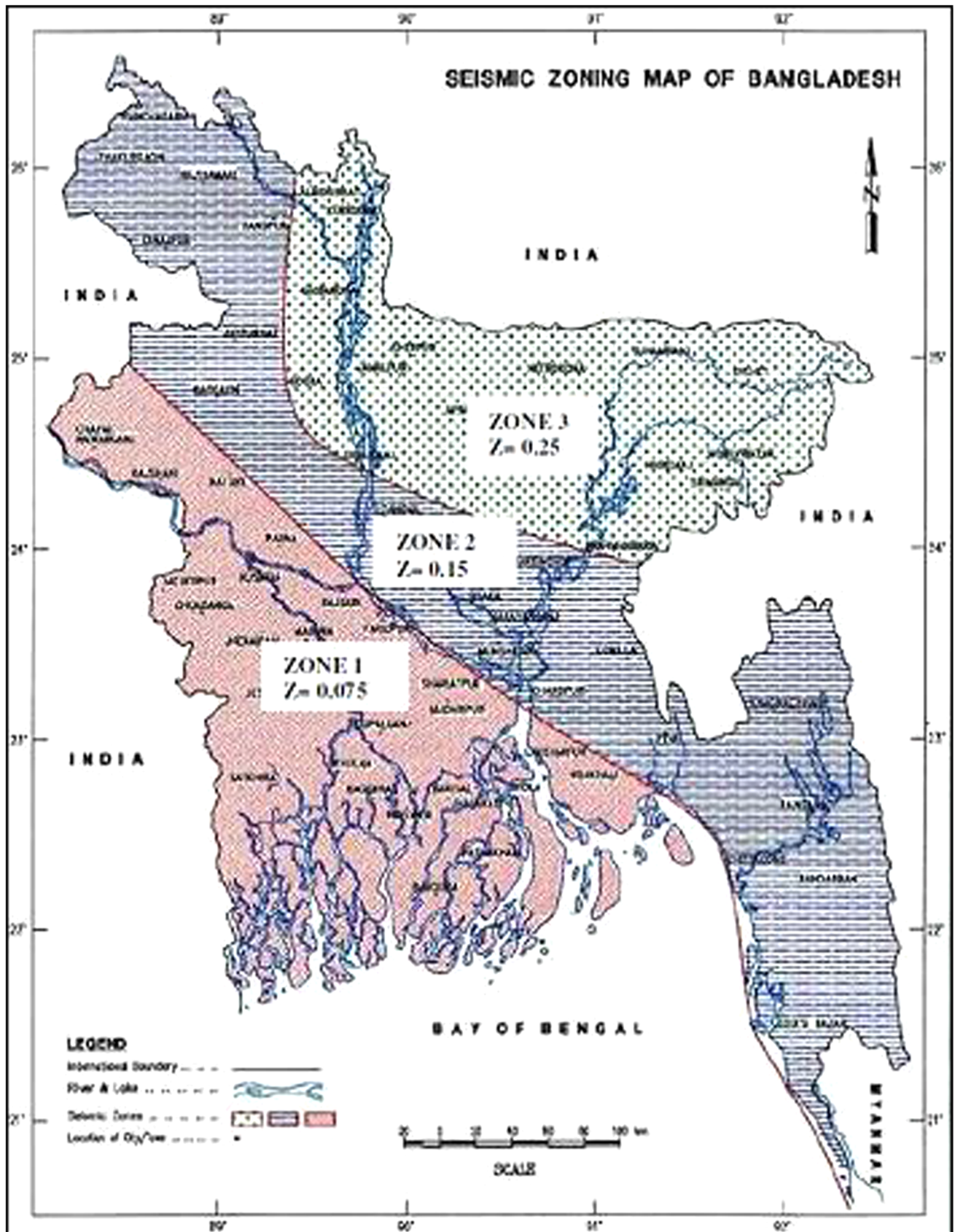
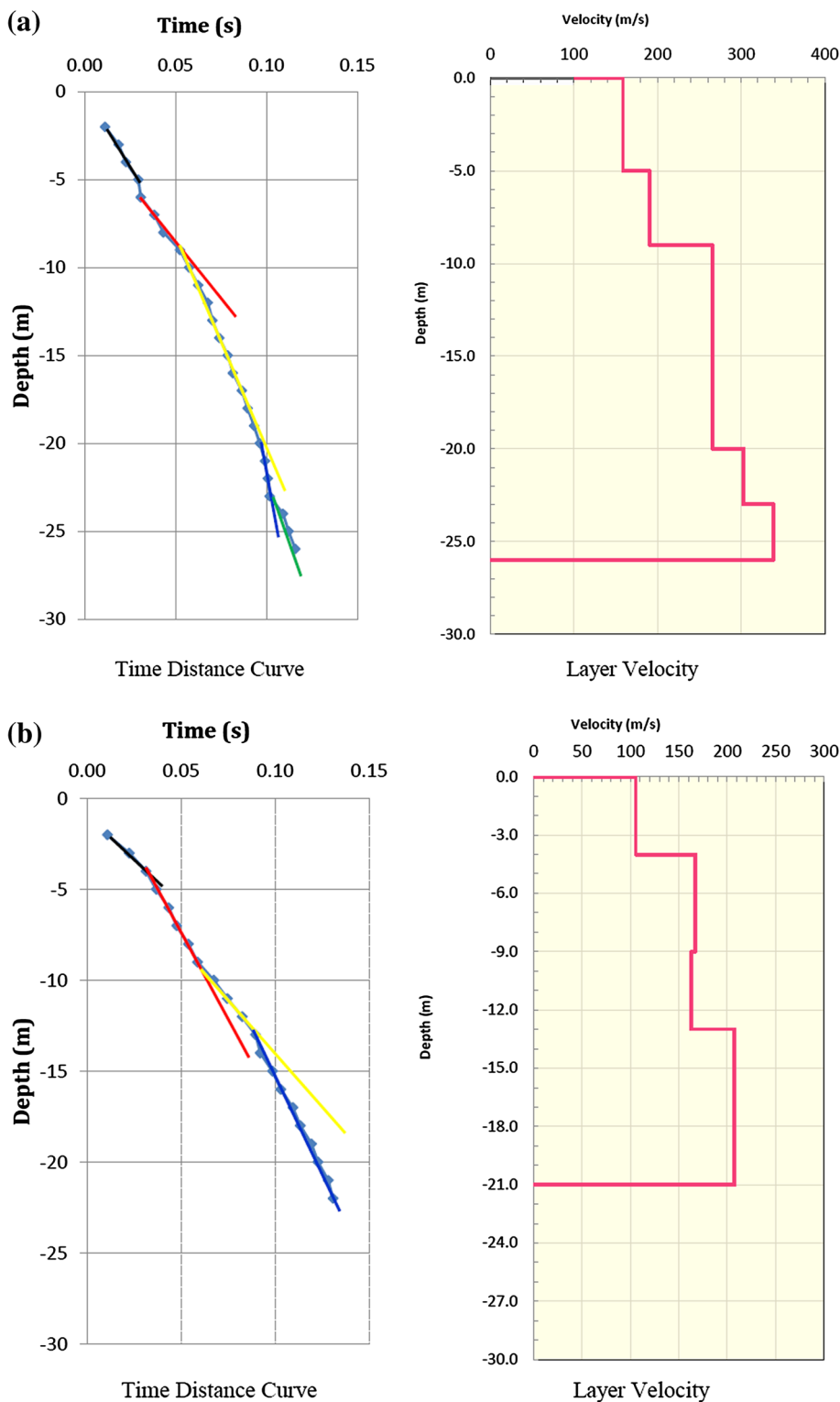


Fig. 7 Seismic zoning map of Bangladesh (BNBC 1993)

Fig. 8 Shear wave velocity (V_s) profiles of PS logging at sites **a** PS-2 and **b** PS-7 in Fig. 2



surface waves (MASW), and microtremor array measurement (MAM) (e.g., Aki 1957; Boore and Brown 1998; Crampin and Bath 1965; Mcmechan and Yedlin 1981; Nazarian et al. 1983; Okada 2003; Park et al. 1999). The V_s

can also be predicted using the empirical correlation between the V_s and SPT-N (e.g., Akin et al. 2011; Imai and Tonouchi 1982; Kuo et al. 2011). In the present study, the V_s was estimated using PS logging, active MASW, and

Table 3 Data acquisition parameters for the MASW survey

Seismic refraction	
Number of channels	24
Geophone spacing	3 m
Array length	69 m
Sampling rate	1 ms
Record length	2 s
Natural frequency of geophone	10 Hz
Source	8-kg hammer
Shot number	25 points, 23 between geophones and 2 outside of measuring line

empirical correlation between the V_s and SPT-N. The AVS30 was then estimated using the V_s of all methods via the following equation:

$$AVS30 = \frac{30}{\sum_{i=1}^N (h_i/v_i)}, \quad (1)$$

where h_i and v_i denote the thickness (in meters) and shear wave of the i th layer, and N denotes the number of layers down to a depth of 30 m.

The AVS30 was estimated at two sites using PS logging, at ten sites using MASW, and at ten sites using SPT-N. Single microtremor measurement was also conducted at 30 sites to determine the predominant period of seismic ground motion.

Shear wave velocity (V_s) estimation using PS logging

PS logging is a direct method for estimating the V_s for seismic site characterization. This test measures the travel time of the elastic wave from the ground surface to various arbitrary depths beneath the surface. The seismic waves were generated by striking a wooden plank using a sledgehammer. The plank was placed on the ground surface 1 m horizontally from the borehole. The waves generated from the plank were received by a triaxial geophone at 1-m intervals from the ground surface to a depth of 30 m in the borehole. The measured travel times (t) of different seismic waves along the inclined path can be corrected to the travel times t_c along the vertical path using the following equation (Auld 1977):

$$t_c = D \frac{t}{R}, \quad (2)$$

where t_c is the corrected travel time, D is the testing depth from the ground surface, t is the first arrival time from the test, and R is the distance between the source and receiver. By plotting the corrected travel time vs. depth, the velocity of each layer can be obtained from the slope of the fitting

Fig. 9 **a** Image of phase velocity (dotted red line is the phase velocity curve). **b** Dispersion curve, **c** one-dimensional shear wave (S-wave) velocity model, and **d** two-dimensional S-wave velocity model at site MASW-5 in Fig. 2

curve using the data points with a similar trend via Eq. (3). The slope of the fitting curve (V_d) represents the wave velocity in each covered range:

$$V_d = \frac{\Delta D}{\Delta t_c}, \quad (3)$$

where ΔD is the depth interval showing a similar slope, and Δt_c is the corrected travel time difference for ΔD .

The V_s profiles determined using PS logging at sites PS-02 and PS-07 in the study area are shown in Fig. 8.

Shear wave velocity (V_s) estimation using MASW

A very popular, more recent method for computing near-surface shear wave velocity estimation is MASW. The MASW seismic surface wave technique is widely used for subsurface site characterization and is increasingly being applied for seismic microzonation and site response studies (Anbazhagan and Sitharam 2008). It is also used for geotechnical site characterization of near-surface materials (Park and Elrick 1998; Park et al. 1999, 2005; Xia et al. 1999). The data acquisition parameters of the MASW survey for the present study are shown in Table 3.

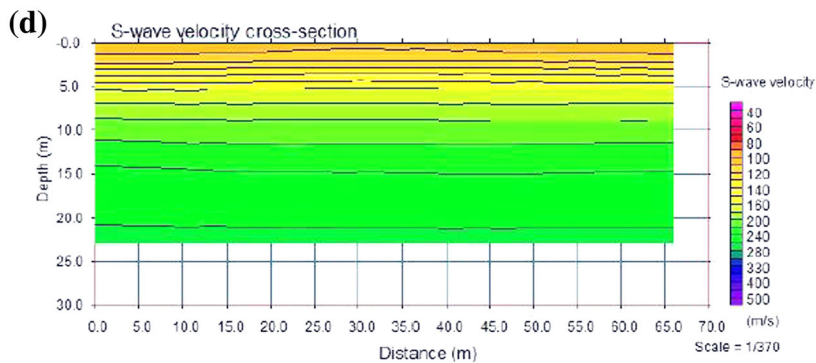
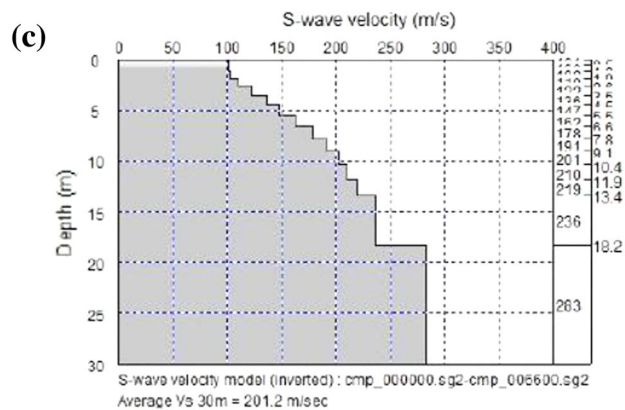
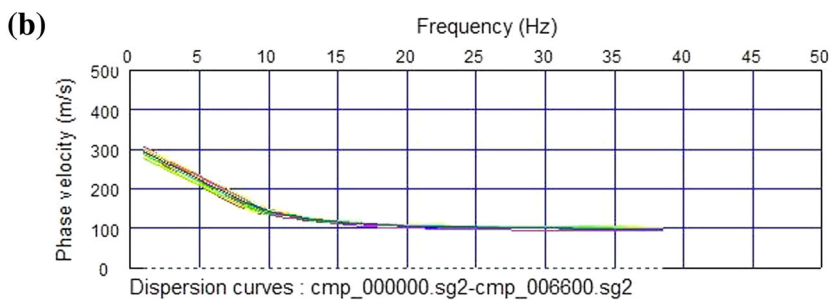
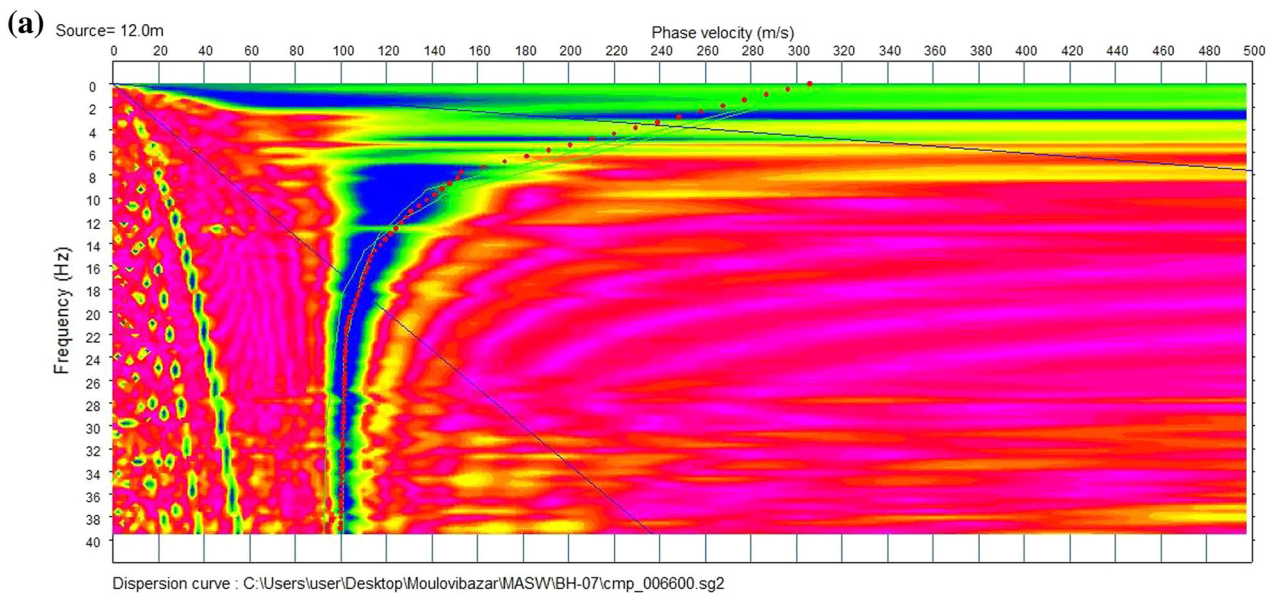
Data processing comprises two main steps: (1) obtaining the dispersion curves of the Rayleigh wave phase velocity from the seismic wave records, and (2) determining the V_s profiles from which the AVS30 value is calculated (Fig. 9). In the phase velocity analysis, the spatial autocorrelation (SPAC) method (Okada 2003) is employed. Spatial autocorrelation function $\rho(\omega, r)$ is expressed by the Bessel function:

$$\rho(\omega, r) = J_0(\omega r/c(\omega)), \quad (4)$$

where r is the distance between receivers, ω is the angular frequency, $c(\omega)$ is the phase velocity of the waves, and J_0 is the first type of Bessel function. The phase velocity was obtained at each frequency using Eq. (4). A one-dimensional inversion using a non-linear least squares method was applied to the phase velocity curves.

Shear wave velocity (V_s) estimation using correlation between V_s and SPT-N

The standard penetration test (SPT) is one of the oldest and most commonly used in situ test methods for site characterization in geotechnical and foundation engineering, because of the simplicity of the equipment and test procedures (Anbazhagan et al. 2012). As such, V_s prediction using standard penetration test blow counts (SPT-N) has



become very popular in geotechnical earthquake engineering. In the present study, SPT was performed at 1.5-m intervals in ten boreholes.

Empirical correlations between the V_s and SPT-N have been proposed by various researchers for different types of soils in different parts of the world (Imai 1977; Ohta and Goto 1978; Imai and Tonouchi 1982; Andrus et al. 2006; Hasaŋebi and Ulusay 2007; Dikmen 2009; Maheswari et al. 2010; Fabbrocino et al. 2015). Hasaŋebi and Ulusay (2007) noted that the SPT-N was a significant parameter in correlations between the V_s and SPT-N, while the type of soil had no important influence. The use of equations for all soils based on the uncorrected SPT-N is appropriate for the indirect estimation of the V_s (Hasaŋebi and Ulusay 2007). Although the use of the SPT in clayey soils is not appropriate, many researchers have used the SPT-N of clayey soils to predict the V_s (e.g., Dikmen 2009; Hasaŋebi and Ulusay 2007; Imai 1977; Lee 1990). However, uncorrected SPT-N data are used in the present study to predict the V_s . As the V_s data that are estimated using PS logging are not sufficient for developing a correlation between the V_s and uncorrected SPT-N, the correlation equation (Eq. 5) for all soils proposed by Maheswari et al. (2010) is used in the present study. The V_s values that are predicted using this equation are close to the V_s estimated using PS logging and MASW (Fig. 10):

$$V_s = 95.64 N^{0.301}, \quad (5)$$

where V_s is the average near-surface shear wave velocity of the soil (m/s) to a depth of 30 m, and N is the uncorrected SPT-N value in the field.

AVS30 estimation and amplification factor

The average near-surface shear wave velocity of soils to a depth of 30 m (AVS30) is directly related to the amplification of ground motion intensity during an earthquake (Matsuoka et al. 2006). Therefore, the AVS30 was estimated using the shear wave velocities (V_s) determined using PS logging, MASW, and SPT-N to determine the amplification factor at different sites within the city (Fig. 10). The amplification factor of the seismic ground motion parameters in the near-surface soils was determined based on the AVS30 according to the NEHRP.

Predominant period estimation using microtremors

Microtremors are a phenomenon of very small ground surface vibrations that occur even during ordinary quiet times as a result of a complex stacking process of

various waves propagating from remote manmade vibration sources such as traffic systems or machinery in industrial plants and from natural vibrations caused by tidal or volcanic activity. Microtremor observations can provide useful information on site dynamic properties such as predominant period and amplitude of seismic waves. These data can be collected easily and cheaply using a portable instrument, thus providing a convenient method for performing seismic microzonation. The predominant period of local soil was estimated using a horizontal/vertical (H/V) spectral ratio of microtremors according to the procedure proposed by Nakamura (1989). The soil response in terms of predominant period and H/V ratio (amplification factor) for several sites is shown in Fig. 11.

Peak ground acceleration (PGA)

The PGA at the engineering base rock of the study area is 0.25 g (Fig. 7), according to the seismic zoning map of Bangladesh (BNBC 1993). It is well known that selection of appropriate PGA for the scenario earthquake may involve uncertainty. The PGA at the ground surface is predicted by multiplying the PGA at the engineering base rock with the amplification factor of the overlying soft soils estimated from the AVS30 of a site according to the NEHRP guidelines.

Depth for deep foundation

The depth for the deep foundation was determined based on the SPT-N value. The sandy soil layer with SPT-N values ≥ 50 was considered the foundation layer for the deep foundation in the study area.

Grid sizes of different maps

Raster maps of different engineering geological and seismic parameters were created using an interpolation technique (Fig. 12). The study area was then divided into 250 m \times 250 m grids, and all calculated parameters of each grid were integrated using zonal statistics (a spatial analysis tool of ArcGIS).

Results and discussion

The average near-surface shear wave velocity to a depth of 30 m (AVS30) is a very important factor in evaluating the subsurface soil dynamics and is essential for seismic

Fig. 10 Average shear wave velocity to a depth of 30 m (AVS30) from shear wave velocity profiles of standard penetration test blow counts (SPT-N), PS logging, and multichannel analysis of surface waves (MASW)

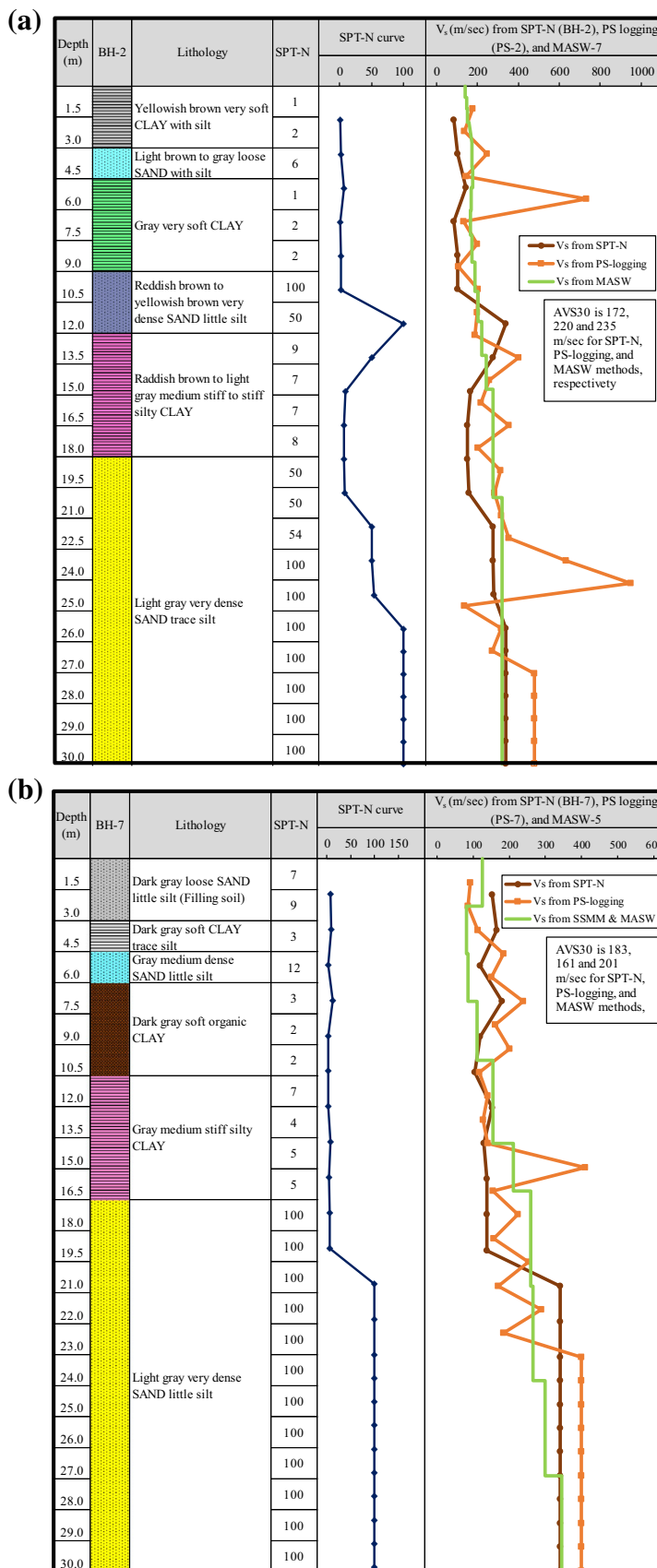
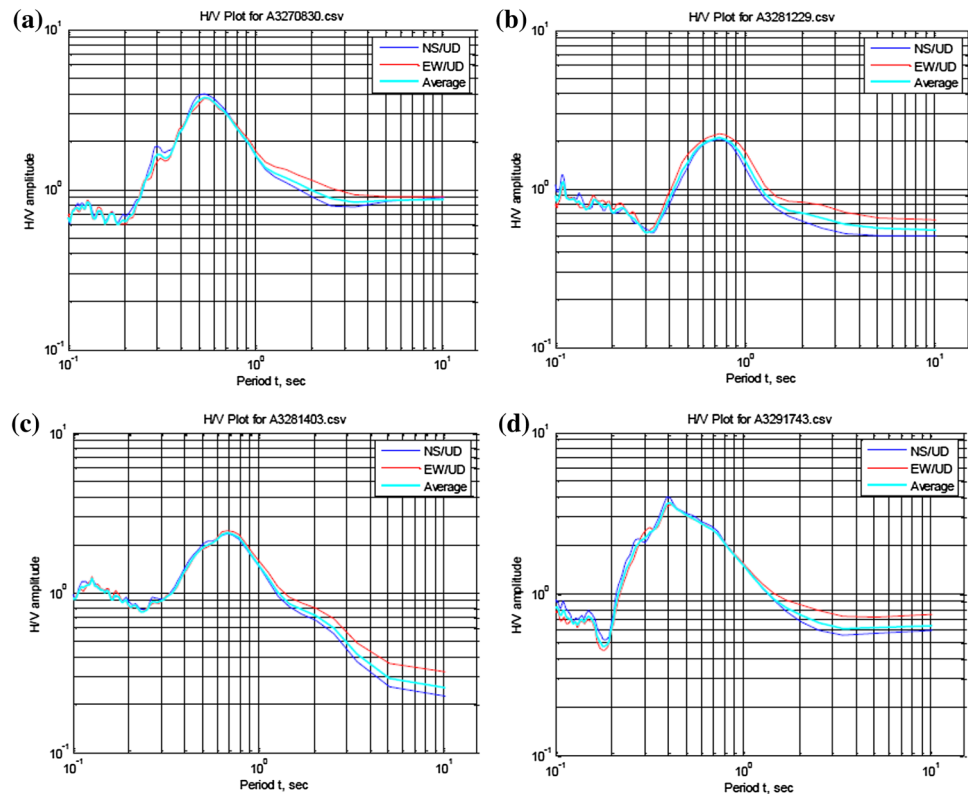


Fig. 11 Soil response in terms of predominant period and amplification factor from microtremor (H/V) records at various sites: **a** 24.48821°N, 91.77347°E (Town Hall Field); **b** 24.48628°N, 91.75043°E (Hilalpur); **c** 24.48129°N, 91.75827°E (Syed Abdul Malik High School); **d** 24.48247°N, 91.77380°E (Khadirgaon)



hazard assessment. The AVS30 in the study area ranged from 150 to 235 m/s (Table 4), and was found to be slightly better in the eastern part than the western part (Fig. 12b). According to the NEHRP classification, the area exhibits mainly two types of soil: stiff soil class D ($180 \text{ m/s} < V_s^{30} < 360 \text{ m/s}$) and soils with soft clay class E ($180 \text{ m/s} > V_s^{30}$) (Fig. 12c). The soil amplification factors (SAF) for type D and E soils are 1.3 and 1.45, respectively (Fig. 12d).

The PGA at the engineering base rock is 0.25 g (Fig. 12e) according to the seismic zoning map of Bangladesh (BNBC 1993), and the PGA at the ground surface of soil types D and E is 0.325 and 0.3625 g, respectively (Fig. 12f).

During fieldwork in the study area, it was observed that some buildings were tilting or had collapsed due to the selection of an improper foundation layer. The foundation depth for the deep foundation was determined at depths from 15 to 29 m (Table 4). In addition, the western part of the study area showed higher foundation depth than the eastern part (Fig. 12g).

The predominant periods of the study area ranged from 0.35 to 0.72 s (Table 4), with the eastern portion showing an approximate range of 0.35 to 0.60 s and the western

portion 0.60 to 0.72 s (Fig. 12h). If the predominant period is known at the site of construction, engineers can design the structure such that the natural period of the structure does not coincide with the predominant period. All parameters at each grid of the study area are shown in Table 4. These parameters will be very helpful for urban planners in developing an earthquake risk-sensitive land use plan to enable the design of earthquake-resistant structures.

Conclusions

A number of geotechnical and geophysical site investigation techniques were used to estimate various parameters of seismic site characterization for the town of Moulvibazar, the capital of Moulvibazar district in Bangladesh. These parameters are essential for urban planning in preparing an earthquake risk-sensitive land use plan for designing earthquake-resistant structures. The study area is characterized as site classes D and E based on the NEHRP system, and exhibits AVS30 of 150–235 m/s, with corresponding soil amplification factors of 1.3 and 1.45, respectively. The predominant periods range from 0.35 to

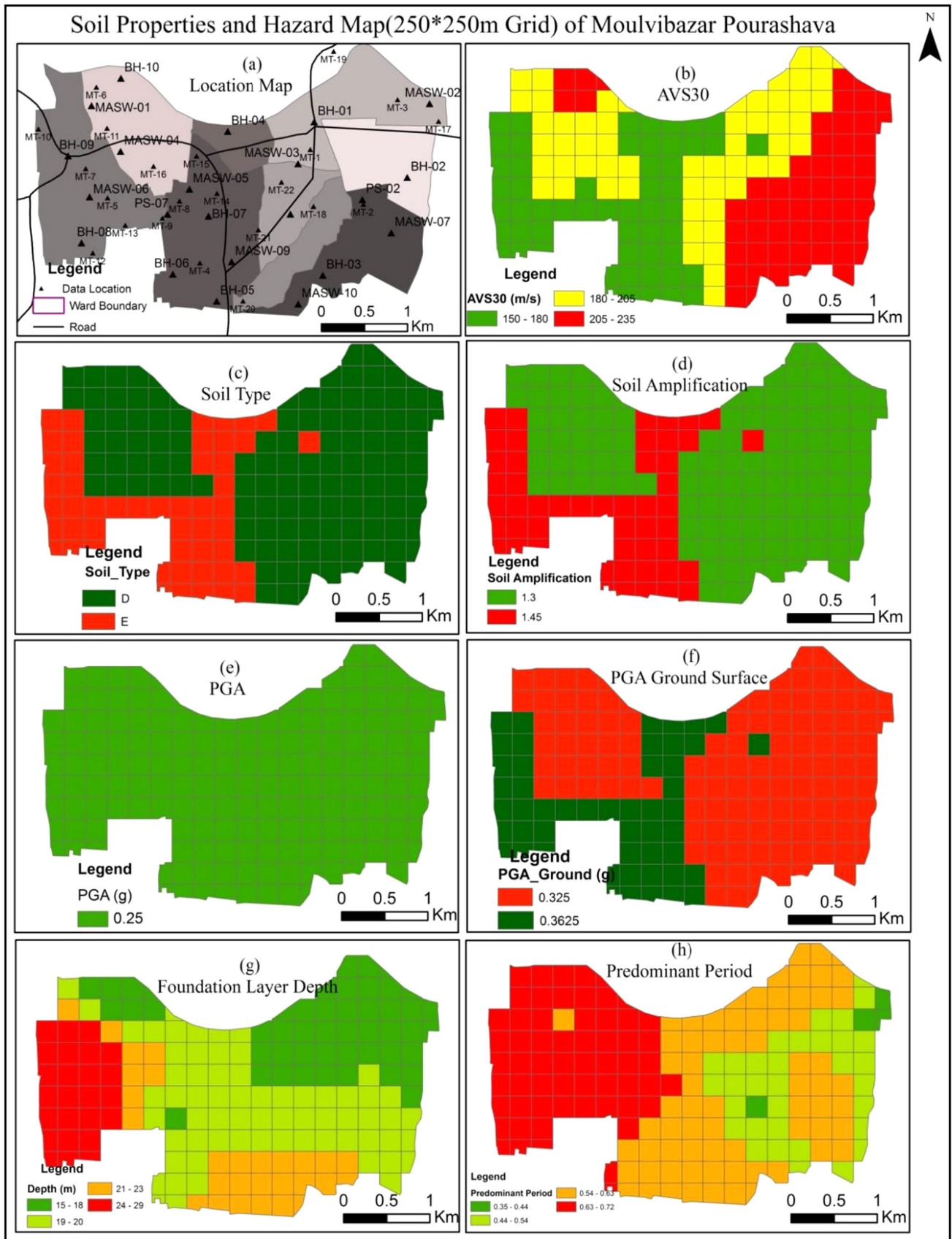


Fig. 12 Different parameter maps of seismic site characterization for Moulvibazar town at a grid size of 250 m × 250 m

Table 4 Different parameters of seismic site characterization for each 250 m × 250 m grid of study area

Grid ID	Coordinates		AVS30 (m/s)	Soil type	Soil amplification	Peak ground acceleration at bedrock (g)	Peak ground acceleration at ground surface	Foundation depth (m) for footing	Predominant period (s)
	Latitude	Longitude							
1	24.4971	91.7780	198	D	1.30	0.25	0.325	17	0.61
2	24.4971	91.7800	200	D	1.30	0.25	0.325	17	0.57
3	24.4965	91.7817	204	D	1.30	0.25	0.325	17	0.55
4	24.4949	91.7487	196	D	1.30	0.25	0.325	20	0.68
5	24.4950	91.7509	204	D	1.30	0.25	0.325	17	0.68
6	24.4950	91.7532	225	D	1.30	0.25	0.325	15	0.67
7	24.4949	91.7553	227	D	1.30	0.25	0.325	15	0.67
8	24.4944	91.7571	210	D	1.30	0.25	0.325	17	0.66
9	24.4947	91.7758	194	D	1.30	0.25	0.325	17	0.59
10	24.4950	91.7779	199	D	1.30	0.25	0.325	17	0.58
11	24.4950	91.7801	203	D	1.30	0.25	0.325	17	0.56
12	24.4949	91.7823	208	D	1.30	0.25	0.325	17	0.56
13	24.4943	91.7843	213	D	1.30	0.25	0.325	17	0.52
14	24.4927	91.7487	189	D	1.30	0.25	0.325	23	0.68
15	24.4927	91.7509	199	D	1.30	0.25	0.325	20	0.67
16	24.4927	91.7532	206	D	1.30	0.25	0.325	18	0.65
17	24.4927	91.7554	207	D	1.30	0.25	0.325	17	0.66
18	24.4927	91.7576	197	D	1.30	0.25	0.325	18	0.66
19	24.4921	91.7594	185	D	1.30	0.25	0.325	19	0.66
20	24.4922	91.7715	183	D	1.30	0.25	0.325	17	0.56
21	24.4927	91.7734	187	D	1.30	0.25	0.325	17	0.56
22	24.4927	91.7756	192	D	1.30	0.25	0.325	17	0.56
23	24.4927	91.7779	199	D	1.30	0.25	0.325	17	0.56
24	24.4927	91.7801	205	D	1.30	0.25	0.325	18	0.55
25	24.4927	91.7824	211	D	1.30	0.25	0.325	18	0.56
26	24.4927	91.7846	216	D	1.30	0.25	0.325	17	0.47
27	24.4926	91.7865	217	D	1.30	0.25	0.325	17	0.39
28	24.4905	91.7464	165	E	1.45	0.25	0.363	27	0.72
29	24.4905	91.7487	171	E	1.45	0.25	0.363	26	0.69
30	24.4905	91.7509	183	D	1.30	0.25	0.325	24	0.64
31	24.4905	91.7532	190	D	1.30	0.25	0.325	21	0.62
32	24.4905	91.7554	191	D	1.30	0.25	0.325	20	0.65
33	24.4905	91.7577	187	D	1.30	0.25	0.325	20	0.66
34	24.4905	91.7599	180	D	1.30	0.25	0.325	19	0.65
35	24.4902	91.7621	169	E	1.45	0.25	0.363	19	0.64
36	24.4900	91.7644	158	E	1.45	0.25	0.363	19	0.62
37	24.4901	91.7667	160	E	1.45	0.25	0.363	19	0.59
38	24.4904	91.7690	175	E	1.45	0.25	0.363	18	0.57
39	24.4905	91.7711	182	D	1.30	0.25	0.325	17	0.55
40	24.4905	91.7734	184	D	1.30	0.25	0.325	16	0.54
41	24.4905	91.7756	188	D	1.30	0.25	0.325	17	0.54
42	24.4905	91.7779	198	D	1.30	0.25	0.325	17	0.54
43	24.4905	91.7801	207	D	1.30	0.25	0.325	18	0.54
44	24.4905	91.7824	212	D	1.30	0.25	0.325	18	0.52
45	24.4905	91.7846	216	D	1.30	0.25	0.325	18	0.42
46	24.4908	91.7865	217	D	1.30	0.25	0.325	17	0.35
47	24.4883	91.7465	154	E	1.45	0.25	0.363	29	0.71

Table 4 continued

Grid ID	Coordinates		AVS30 (m/s)	Soil type	Soil amplification	Peak ground acceleration at bedrock (g)	Peak ground acceleration at ground surface	Foundation depth (m) for footing	Predominant period (s)
	Latitude	Longitude							
48	24.4882	91.7487	151	E	1.45	0.25	0.363	29	0.70
49	24.4882	91.7509	183	D	1.30	0.25	0.325	27	0.68
50	24.4882	91.7532	184	D	1.30	0.25	0.325	24	0.66
51	24.4882	91.7554	183	D	1.30	0.25	0.325	22	0.67
52	24.4882	91.7577	182	D	1.30	0.25	0.325	21	0.67
53	24.4882	91.7599	180	D	1.30	0.25	0.325	20	0.65
54	24.4882	91.7621	174	E	1.45	0.25	0.363	20	0.64
55	24.4882	91.7644	169	E	1.45	0.25	0.363	19	0.62
56	24.4882	91.7666	173	E	1.45	0.25	0.363	19	0.59
57	24.4882	91.7689	180	D	1.30	0.25	0.325	18	0.55
58	24.4882	91.7711	182	D	1.30	0.25	0.325	17	0.54
59	24.4882	91.7734	178	E	1.45	0.25	0.363	16	0.54
60	24.4882	91.7756	186	D	1.30	0.25	0.325	17	0.54
61	24.4882	91.7779	201	D	1.30	0.25	0.325	18	0.54
62	24.4882	91.7801	210	D	1.30	0.25	0.325	18	0.53
63	24.4882	91.7824	213	D	1.30	0.25	0.325	18	0.51
64	24.4882	91.7846	215	D	1.30	0.25	0.325	18	0.45
65	24.4860	91.7466	158	E	1.45	0.25	0.363	28	0.70
66	24.4860	91.7487	160	E	1.45	0.25	0.363	29	0.71
67	24.4860	91.7509	182	D	1.30	0.25	0.325	27	0.72
68	24.4860	91.7532	183	D	1.30	0.25	0.325	24	0.69
69	24.4860	91.7554	181	D	1.30	0.25	0.325	22	0.68
70	24.4860	91.7577	183	D	1.30	0.25	0.325	21	0.68
71	24.4860	91.7599	183	D	1.30	0.25	0.325	20	0.66
72	24.4860	91.7621	179	E	1.45	0.25	0.363	20	0.64
73	24.4860	91.7644	177	E	1.45	0.25	0.363	19	0.63
74	24.4860	91.7666	182	D	1.30	0.25	0.325	19	0.59
75	24.4860	91.7689	188	D	1.30	0.25	0.325	18	0.53
76	24.4860	91.7711	189	D	1.30	0.25	0.325	18	0.51
77	24.4860	91.7734	188	D	1.30	0.25	0.325	17	0.51
78	24.4860	91.7756	199	D	1.30	0.25	0.325	18	0.52
79	24.4860	91.7779	212	D	1.30	0.25	0.325	18	0.54
80	24.4860	91.7801	218	D	1.30	0.25	0.325	19	0.54
81	24.4860	91.7824	217	D	1.30	0.25	0.325	18	0.52
82	24.4860	91.7846	216	D	1.30	0.25	0.325	18	0.49
83	24.4838	91.7466	166	E	1.45	0.25	0.363	27	0.70
84	24.4838	91.7487	172	E	1.45	0.25	0.363	27	0.70
85	24.4838	91.7509	183	D	1.30	0.25	0.325	26	0.69
86	24.4838	91.7532	185	D	1.30	0.25	0.325	25	0.68
87	24.4838	91.7554	180	D	1.30	0.25	0.325	22	0.68
88	24.4838	91.7577	188	D	1.30	0.25	0.325	20	0.68
89	24.4838	91.7599	190	D	1.30	0.25	0.325	19	0.67
90	24.4838	91.7621	180	D	1.30	0.25	0.325	20	0.65
91	24.4838	91.7644	178	E	1.45	0.25	0.363	20	0.63
92	24.4838	91.7666	186	D	1.30	0.25	0.325	19	0.59
93	24.4838	91.7689	195	D	1.30	0.25	0.325	19	0.53
94	24.4838	91.7711	203	D	1.30	0.25	0.325	19	0.50

Table 4 continued

Grid ID	Coordinates		AVS30 (m/s)	Soil type	Soil amplification	Peak ground acceleration at bedrock (g)	Peak ground acceleration at ground surface	Foundation depth (m) for footing	Predominant period (s)
	Latitude	Longitude							
95	24.4838	91.7734	210	D	1.30	0.25	0.325	19	0.46
96	24.4838	91.7756	216	D	1.30	0.25	0.325	19	0.49
97	24.4838	91.7779	222	D	1.30	0.25	0.325	19	0.57
98	24.4838	91.7801	225	D	1.30	0.25	0.325	19	0.58
99	24.4838	91.7824	222	D	1.30	0.25	0.325	19	0.55
100	24.4838	91.7846	218	D	1.30	0.25	0.325	18	0.52
101	24.4815	91.7466	169	E	1.45	0.25	0.363	26	0.69
102	24.4815	91.7487	172	E	1.45	0.25	0.363	26	0.69
103	24.4815	91.7509	177	E	1.45	0.25	0.363	27	0.69
104	24.4815	91.7532	174	E	1.45	0.25	0.363	27	0.70
105	24.4815	91.7554	173	E	1.45	0.25	0.363	23	0.70
106	24.4815	91.7576	173	E	1.45	0.25	0.363	19	0.68
107	24.4815	91.7599	174	E	1.45	0.25	0.363	18	0.67
108	24.4815	91.7621	177	E	1.45	0.25	0.363	19	0.64
109	24.4815	91.7644	179	E	1.45	0.25	0.363	20	0.62
110	24.4815	91.7666	188	D	1.30	0.25	0.325	20	0.58
111	24.4815	91.7689	201	D	1.30	0.25	0.325	20	0.56
112	24.4815	91.7711	215	D	1.30	0.25	0.325	19	0.51
113	24.4815	91.7734	229	D	1.30	0.25	0.325	19	0.44
114	24.4815	91.7756	228	D	1.30	0.25	0.325	19	0.48
115	24.4815	91.7779	226	D	1.30	0.25	0.325	19	0.57
116	24.4815	91.7801	227	D	1.30	0.25	0.325	19	0.58
117	24.4815	91.7824	223	D	1.30	0.25	0.325	19	0.55
118	24.4816	91.7845	220	D	1.30	0.25	0.325	19	0.53
119	24.4793	91.7468	168	E	1.45	0.25	0.363	26	0.69
120	24.4793	91.7487	167	E	1.45	0.25	0.363	26	0.68
121	24.4793	91.7509	159	E	1.45	0.25	0.363	28	0.68
122	24.4793	91.7599	170	E	1.45	0.25	0.363	19	0.64
123	24.4793	91.7621	174	E	1.45	0.25	0.363	20	0.61
124	24.4793	91.7644	178	E	1.45	0.25	0.363	20	0.59
125	24.4793	91.7666	188	D	1.30	0.25	0.325	20	0.57
126	24.4793	91.7689	204	D	1.30	0.25	0.325	20	0.56
127	24.4793	91.7711	218	D	1.30	0.25	0.325	20	0.54
128	24.4793	91.7734	231	D	1.30	0.25	0.325	20	0.51
129	24.4793	91.7756	230	D	1.30	0.25	0.325	20	0.51
130	24.4793	91.7779	226	D	1.30	0.25	0.325	20	0.54
131	24.4793	91.7801	224	D	1.30	0.25	0.325	19	0.55
132	24.4793	91.7824	222	D	1.30	0.25	0.325	19	0.54
133	24.4793	91.7842	221	D	1.30	0.25	0.325	19	0.54
134	24.4774	91.7469	166	E	1.45	0.25	0.363	25	0.68
135	24.4775	91.7486	164	E	1.45	0.25	0.363	26	0.68
136	24.4777	91.7509	158	E	1.45	0.25	0.363	28	0.68
137	24.4770	91.7599	165	E	1.45	0.25	0.363	20	0.60
138	24.4770	91.7621	172	E	1.45	0.25	0.363	20	0.55
139	24.4770	91.7644	175	E	1.45	0.25	0.363	21	0.57
140	24.4770	91.7666	186	D	1.30	0.25	0.325	21	0.57
141	24.4770	91.7689	202	D	1.30	0.25	0.325	21	0.56

Table 4 continued

Grid ID	Coordinates		AVS30 (m/s)	Soil type	Soil amplification	Peak ground acceleration at bedrock (g)	Peak ground acceleration at ground surface	Foundation depth (m) for footing	Predominant period (s)
	Latitude	Longitude							
142	24.4770	91.7711	218	D	1.30	0.25	0.325	21	0.55
143	24.4770	91.7734	228	D	1.30	0.25	0.325	22	0.54
144	24.4770	91.7756	229	D	1.30	0.25	0.325	21	0.53
145	24.4770	91.7779	227	D	1.30	0.25	0.325	21	0.53
146	24.4770	91.7801	224	D	1.30	0.25	0.325	20	0.54
147	24.4770	91.7824	222	D	1.30	0.25	0.325	20	0.54
148	24.4771	91.7842	221	D	1.30	0.25	0.325	20	0.53
149	24.4747	91.7581	162	E	1.45	0.25	0.363	20	0.63
150	24.4748	91.7599	163	E	1.45	0.25	0.363	19	0.60
151	24.4748	91.7621	170	E	1.45	0.25	0.363	20	0.57
152	24.4748	91.7644	172	E	1.45	0.25	0.363	21	0.56
153	24.4748	91.7666	180	E	1.45	0.25	0.363	21	0.55
154	24.4748	91.7689	199	D	1.30	0.25	0.325	21	0.55
155	24.4748	91.7711	220	D	1.30	0.25	0.325	22	0.55
156	24.4749	91.7733	232	D	1.30	0.25	0.325	22	0.55
157	24.4748	91.7757	234	D	1.30	0.25	0.325	22	0.54
158	24.4753	91.7778	229	D	1.30	0.25	0.325	21	0.53
159	24.4750	91.7825	222	D	1.30	0.25	0.325	20	0.54
160	24.4733	91.7581	165	E	1.45	0.25	0.363	20	0.63
161	24.4730	91.7599	167	E	1.45	0.25	0.363	20	0.60
162	24.4729	91.7621	169	E	1.45	0.25	0.363	21	0.58
163	24.4729	91.7644	164	E	1.45	0.25	0.363	22	0.56
164	24.4727	91.7666	167	E	1.45	0.25	0.363	22	0.54
165	24.4726	91.7689	193	D	1.30	0.25	0.325	22	0.55
166	24.4726	91.7712	221	D	1.30	0.25	0.325	22	0.56
167	24.4728	91.7727	235	D	1.30	0.25	0.325	22	0.55

0.72 s, with PGA at the surface of 0.325 and 0.3625 g, and foundation depth for deep foundation of 15–29 m. The uncertainties associated with this study are due to a small number of SPT profiles, PS logging, and MASW surveys.

The PGA at the base rock was not determined using suitable ground motion prediction equations and earthquake sources. It was taken from the existing earthquake zoning map of Bangladesh published in the Bangladesh National Building Code (BNBC 1993). The earthquake zoning map of Bangladesh needs to be revised using updated data and seismic hazard analysis methodologies. Therefore, the prediction of PGA at the base rock is also uncertain for determining the PGA at the ground surface.

Acknowledgements The authors would like to thank the Ministry of Science and Technology (MoST) for providing financial support for this research project through a special allocation. The authors are also grateful to Moulvibazar local administrative authorities for their support during data acquisition, and to Mr. Md. Ashraful Islam, Assistant Professor, Department of Geology, and Dewan Md. Enamul Haque, Lecturer, and BM Rabby Hossain, Lecturer, Department of

Disaster Science and Management, University of Dhaka, for their support in completing this research.

References

- Abrahamson NA, Silva W, Kamai R (2013) Update of the AS08 Ground-Motion Prediction equations based on the NGA-West2 data set. Pacific Engineering Research Center Report 174
- Acharyya SK (2007) Collisional emplacement history of the Naga-Andaman ophiolites and the position of the eastern Indian suture. *J Asian Earth Sci* 29:229–242. doi:10.1016/j.jseae.2006.03.003
- Aitchison JC, Ali JR, Davis AM (2007) When and where did India and Asia collide? *J Geophys Res* 112:1978–2012
- Aki K (1957) Space and time spectra of stationary stochastic waves, with special reference to microtremors. *Bull Earthq Res Inst* 35:415–456
- Akin MK, Kramer SL, Topal T (2011) Empirical correlations of shear wave velocity (V_s) and penetration resistance (SPT-N) for different soils in an earthquake-prone area (Erbaa-Turkey). *Eng Geol* 119:1–17. doi:10.1016/j.enggeo.2011.01.007
- Alam M, Alam MM, Curray JR (2003) An overview of the sedimentary geology of the Bengal Basin in relation to the

- regional tectonic framework and basin-fill history. *Sed Geol* 155:179–208
- Ambraseys NN, Douglas J (2004) Magnitude calibration of north Indian earthquakes. *Geophys J Int* 159:165–206. doi:10.1111/j.1365-246X.2004.02323.x
- Anbazhagan P, Sitharam TG (2008) Mapping of average shear wave velocity for Bangalore region: a case study. *J Environ Eng Geophys* 13:69–84. doi:10.2113/JEEG13.2.69
- Anbazhagan P, Parihar A, Rashmi HN (2012) Review of correlations between SPT N and shear modulus: a new correlation applicable to any region. *Soil Dyn Earthq Eng* 36:52–69. doi:10.1016/j.soildyn.2012.01.005
- Anderson JG, Lee Y, Zeng Y, Day S (1996) Control of strong motion by the upper 30 meters. *Bull Seismol Soc Am* 86:1749–1759
- Andrus RD, Fairbanks CD, Zhang J et al (2006) Shear-wave velocity and seismic response of near-surface sediments in Charleston, South Carolina. *Bull Seismol Soc Am* 96:1897–1914
- Auld B (1977) Cross-hole and down-hole Vs by mechanical impulse. *J Geotech Eng Div* 103:1381–1398
- Benjumea B, Hunter JA, Pullan SE, et al (2008) Vs30 and fundamental site period estimates in soft sediments of the Ottawa Valley from near-surface geophysical measurements. *J Environ Eng Geophys* 13(4):313–323. doi: 10.2113/JEEG13.4.313
- Bilham R (2004) Earthquakes in India and the Himalaya: tectonics, geodesy and history. *Ann Geophys* 47:839–858. doi:10.4401/ag-3338
- Bilham R, England P (2001) Plateau “pop-up” in the great 1897 Assam earthquake. *Nature* 410:806–809. doi:10.1038/35071057
- Bilham R, Hough S (2006) Future earthquakes on the Indian subcontinent: inevitable hazard, preventable risk. *South Asian J* 12:1–9
- BNBC (1993) Bangladesh national building codes (BNBC). Housing and Building Research Institute and Bangladesh Standards and Testing Institution, Dhaka
- Boore DM, Brown LT (1998) Comparing shear-wave velocity profiles from inversion of surface-wave phase velocities with downhole measurements: systematic differences between the CXW method and downhole measurements at six USC strong-motion sites. *Seismol Res Lett* 69:222–229. doi:10.1785/gssrl.69.3.222
- Boore DM, Stewart J, Seyhan E, Atkinson GM (2013) NGA-West2 Equations for Predicting Response Spectral Accelerations for Shallow Crustal Earthquakes. doi:10.1193/070113EQS184M
- Borcherdt RD (1994) Estimates of site-dependent response spectra for design. *Earthq Spectra* 10:617–653
- Brandenberg SJ, Bellana N, Shantz T (2010) Shear wave velocity as function of standard penetration test resistance and vertical effective stress at California bridge sites. *Soil Dyn Earthq Eng* 30:1026–1035. doi:10.1016/j.soildyn.2010.04.014
- BSSC (2015) NEHRP recommended seismic provisions for new buildings and other structures. Part 1 (provisions) and Part 2 (commentary), FEMA P-1050-1, Building Seismic Safety Council, Federal Emergency Management Agency, Washington, D.C.
- Campbell KW, Bozorgnia Y (2013) NGA-West2 Campbell-Bozorgnia ground motion model for the horizontal components of PGA, PGV, response spectra for periods ranging from 0.01 to 10 sec
- Castelli F, Cavallaro A, Grasso S, Lentini V (2016) Seismic microzoning from synthetic ground motion earthquake scenarios parameters: the case study of the city of Catania (Italy). 88:307–327. doi:10.1016/j.soildyn.2016.07.010
- Cavallaro A, Grasso S, Maugeri M (2006) Volcanic soil characterisation and site response analysis in the City of Catania. In: Proceedings of the 8th National Conference on Earthquake Engineering. San Francisco, April 18–22, 2006, pp 835–844
- Cavallaro A, Grasso S, Maugeri M (2008) Site Response Analysis for Tito Scalo Area (PZ) in the Basilicata Region, Italy. In: Proceedings of the 4th Geotechnical Earthquake Engineering and Soil Dynamics Conference. ASCE—Geotechnical Special Publication, Sacramento, May 18–22, 2008, pp 1–11
- Chiou BJS, Youngs RR (2013) Update of the Chiou and Youngs NGA ground motion model for average horizontal component of peak ground motion and response spectra. *Peer Rep* 30:1117–1153. doi:10.1193/1.2894832
- Crampin S, Bath M (1965) Higher modes of seismic surface waves: mode separation. *Geophys J Int* 10:81–92. doi:10.1111/j.1365-246X.1965.tb03053.x
- Curray JR, Emmel FJ, Moore DG, Raitt RW (1982) Structure, tectonics, and geological history of the northeastern Indian Ocean. In: Nairn AEM, Stehli FG (eds) The oceans basins and margins. Plenum, New York, pp 399–449
- Dikmen Ü (2009) Statistical correlations of shear wave velocity and penetration resistance for soils. *J Geophys Eng* 6:61–72. doi:10.1088/1742-2132/7/1/N02
- Dobry R, Borcherdt RD, Crouse CB et al (2000) New site coefficients and site classification system used in recent building seismic code provisions. *Earthq Spectra* 16:41–67
- Eker AM, Akgün H, Koçkar MK (2012) Local site characterization and seismic zonation study by utilizing active and passive surface wave methods: a case study for the northern side of Ankara, Turkey. *Eng Geol* 151:64–81. doi:10.1016/j.enggeo.2012.09.002
- Fabbrocino S, Lanzano G, Forte G et al (2015) SPT blow count vs. shear wave velocity relationship in the structurally complex formations of the Molise Region (Italy). *Eng Geol* 187:84–97. doi:10.1016/j.enggeo.2014.12.016
- Hasançebi N, Ulusay R (2007) Empirical correlations between shear wave velocity and penetration resistance for ground shaking assessments. *Bull Eng Geol Environ* 66:203–213
- Imai T (1977) P and S wave velocities of the ground in Japan. In: Proceeding of IX International Conference on Soil Mechanics and Foundation Engineering, pp 127–132
- Imai T, Tonouchi K (1982) Correlation of N-value with S-wave velocity and shear modulus. In: Proceedings of the 2nd European Symposium of Penetration Testing. Amsterdam, pp 57–72
- Kuo CH, Wen KL, Hsieh HH et al (2011) Evaluating empirical regression equations for Vs and estimating Vs30 in northeastern Taiwan. *Soil Dyn Earthq Eng* 31:431–439. doi:10.1016/j.soildyn.2010.09.012
- Kuo CH, Wen KL, Hsieh HH et al (2012) Site classification and Vs30 estimation of free-field TSMIP stations using the logging data of EGD. *Eng Geol* 129–130:68–75. doi:10.1016/j.enggeo.2012.01.013
- Lee SH (1990) Regression models of shear wave velocities. *J Chin Inst Eng* 13:519–532
- Maheswari RU, Boominathan A, Dodagoudar GR (2010) Use of surface waves in statistical correlations of shear wave velocity and penetration resistance of Chennai soils. *Geotech Geol Eng* 28:119–137. doi:10.1007/s10706-009-9285-9
- Martin S, Szeliga W (2010) A catalog of felt intensity data for 570 earthquakes in India from 1636 to 2009. *Bull Seismol Soc Am* 100:562–569. doi:10.1785/0120080328
- Matsuoka M, Wakamatsu K, Fujimoto K, Midorikawa S (2006) Average shear-wave velocity mapping using Japan engineering geomorphologic classification map. *Struct Eng Earthq Eng* 23:57s–68s. doi:10.2208/jscseeee.23.57s
- Maurin T, Rangin C (2009) Structure and kinematics of the Indo-Burmese Wedge: recent and fast growth of the outer wedge. *Tectonics* 28:1–21. doi:10.1029/2008TC002276
- Mcmehan GA, Yedlin MJ (1981) Analysis of dispersive waves by wave field transformation. *Geophysics* 46:869–874
- Morino M, Kamal ASMM, Muslim D et al (2011) Seismic event of the Dauki Fault in 16th century confirmed by trench

- investigation at Gabrakhari village, Haluaghat, Mymensingh, Bangladesh. *J Asian Earth Sci* 42:492–498. doi:[10.1016/j.jseaes.2011.05.002](https://doi.org/10.1016/j.jseaes.2011.05.002)
- Morino M, Kamal ASMM, Akhter SH et al (2014) A paleoseismological study of the Dauki fault at Jaflong, Sylhet, Bangladesh: historical seismic events and an attempted rupture segmentation model. *J Asian Earth Sci* 91:218–226. doi:[10.1016/j.jseaes.2014.06.002](https://doi.org/10.1016/j.jseaes.2014.06.002)
- Nakamura Y (1989) A method for dynamic characteristics estimation of subsurface using microtremor on the ground surface. Quarterly Report of Railway Technical Research Institute (RTRI) 30(1), Japan
- Nazarian S, Stokoe KHI, Hudson WR (1983) Use of spectral analysis of surface waves method for determination of moduli and thicknesses of pavement systems: transport. *Res Record* 930:38–45
- Ohta Y, Goto N (1978) Empirical shear wave velocity equations in terms of characteristics soil indexes. *Earthq Eng Struct Dynam* 6:167–187
- Okada H (2003) The microtremor survey method. *Geophys Monogr Ser*, SEG
- Oldham RD (1899) Report on the great earthquake of 12th June 1897. *Mem Geol Surv, India*, p 29
- Park S, Elrick S (1998) Predictions of shear-wave velocities in southern California using surface geology. *Bull Seismol Soc Am* 88:677–685
- Park C, Park CB, Miller RD et al (1999) Multichannel analysis of surface waves. *Geophysics* 64:800–808. doi:[10.1190/1.1444590](https://doi.org/10.1190/1.1444590)
- Park C-B, Miller R-D, Ryden N et al (2005) Combined use of active and passive surface waves. *J Environ Eng Geophys* 10:323–334. doi:[10.2113/JEEG10.3.323](https://doi.org/10.2113/JEEG10.3.323)
- Rahman MZ, Siddiqua S, Kamal ASMM (2015) Liquefaction hazard mapping by liquefaction potential index for Dhaka City, Bangladesh. *Eng Geol* 188:137–147. doi:[10.1016/j.enggeo.2015.01.012](https://doi.org/10.1016/j.enggeo.2015.01.012)
- Rahman MZ, Siddiqua S, Kamal ASMM (2016) Shear wave velocity estimation of the near-surface materials of Chittagong City. *J Appl Geophys, Bangladesh for seismic site characterization*. doi:[10.1016/j.jappgeo.2016.09.006](https://doi.org/10.1016/j.jappgeo.2016.09.006)
- Steckler MS, Akhter SH, Seeber L (2008) Collision of the Ganges-Brahmaputra Delta with the Burma Arc: implications for earthquake hazard. *Earth Planet Sci Lett* 273:367–378. doi:[10.1016/j.epsl.2008.07.009](https://doi.org/10.1016/j.epsl.2008.07.009)
- Stuart M (1920) The Srimangal earthquake of 8th July 1918. *Mem Geol Surv India* 46(1):1–70
- Szeliga W, Hough S, Martin S, Bilham R (2010) Intensity, magnitude, location, and attenuation in India for felt earthquakes since 1762. *Bull Seismol Soc Am* 100:570–584. doi:[10.1785/0120080329](https://doi.org/10.1785/0120080329)
- UBC (1997) International conference of building officials. Uniform Building Code, Whittier
- Xia J, Miller RD, Park CB (1999) Estimation of near-surface shear wave velocity by inversion of Rayleigh waves. *Geophysics* 64:691–700. doi:[10.1190/1.1444578](https://doi.org/10.1190/1.1444578)